Continuous Variable Entanglement in an Optical Parametric Oscillator Based on a Nondegenerate Four Wave Mixing Process in Hot Alkali Atoms

A. Montaña Guerrero,[1,*] R. L. Rincón Celis,[1] P. Nussenzveig,[1] M. Martinelli,[1] A. M. Marino,[2] and H. M. Florez[1,†]
[1]Instituto de Física, Universidade de São Paulo, 05315-970 São Paulo, SP, Brazil
[2]Center for Quantum Research and Technology and Homer L. Dodge Department of Physics and Astronomy, The University of Oklahoma, Norman, Oklahoma 73019, USA

(Received 26 April 2022; accepted 14 September 2022; published 11 October 2022)

We present the measurement of entanglement between twin beams generated with a doubly resonant optical parameter oscillator (OPO) based on four-wave mixing in hot ^{85}Rb vapor above threshold. This is the first measurement of entanglement in an OPO with a $\chi^{(3)}$ media above threshold. We reconstruct the covariance matrix for several configurations and based on a full picture of the four side band mode state, we study entanglement between all possible bipartitions. We show a robust generation of entanglement with stronger generation for a specific pair of modes. For this system, we show that atomic density is a determinant factor for the generation and loss of quantum correlations. The generation of entangled fields with an atomic OPO operating close to atomic resonance of alkali atoms enables a natural integration into quantum networks.

DOI: 10.1103/PhysRevLett.129.163601

Entanglement, an important quantum phenomena, is a keystone for the development of a quantum network that can be used for quantum communication and quantum computation [1]. Among the diversity of quantum entanglement sources, those in the continuous variable domain have shown great potential for applications and versatility for the generation of entangled states. Specifically, solid-state optical parametric oscillators (OPOs) based on a $\chi^{(2)}$ media have been used to generate correlated and entangled light beams below [2] and above [3] the OPO oscillation threshold. OPOs also have the capability of generation of large ensembles of multimode entangled fields [4–7]. Furthermore, OPOs based on optical chips have been engineered to generate quantum correlated light based on the $\chi^{(3)}$ process of four-wave mixing (FWM) [8] below the oscillation threshold.

Quantum correlated light can also be generated through a free space FWM process in hot atomic vapors [9,10]. These systems present higher gains than their solid-state counterpart, hence a higher efficiency and stronger correlations are expected in both the amplitude and phase quadratures. As a result, FWM offers a promising approach for the construction of OPOs with interesting quantum features, as we have recently demonstrated through the generation of twin beams with an intensity difference squeezing of −2.7 dB [11].

In this Letter, we demonstrate the first measurement (to the best of our knowledge) of entanglement between twin beams generated by a doubly resonant OPO operating above threshold using a $\chi^{(3)}$ media. The amplifying process comes from a FWM process in a hot vapor cell of ^{85}Rb atoms within a cavity. We present a detailed study of the structure of entanglement involving four distinct frequency modes of the field in a basic setup consisting of a pump and a lossy resonant cavity surrounding the gain medium. This basic structure is consistent with a simple model for the OPO [12]. However, due to the fact that we use a cavity of extremely low finesse with a gain medium that can be engineered with the creative use of driving and pump fields [13], our Letter opens the possibility to develop distinct structures of entanglement by playing with the longitudinal modes [4,14] of the cavity. These entangled modes, close to atomic resonance, will provide a useful test bed for quantum information processing including atomic systems as quantum memories [15].

The entanglement between a pair of two modes a and b can be initially verified by the Duan *et al.* [16] criterion, where we compute the sum and difference of the amplitude $\hat{p}$ and phase $\hat{q}$ quadratures of the intense beams, such that $\hat{p}_- = (\hat{p}_a - \hat{p}_b)/\sqrt{2}$ and $\hat{q}_+ = (\hat{q}_a + \hat{q}_b)/\sqrt{2}$. A violation of the inequality

$$\Delta^2 \hat{p}_- + \Delta^2 \hat{q}_+ \geq 2 \tag{1}$$

demonstrates a continuous variable entangled state. This corresponds to the quantum correlations involving the two intense output beams generated by the OPO, considering a given analysis frequency of the detected photocurrents. Nevertheless, a richer frequency mode structure is present in the detailed treatment of these photocurrents [17]. Photodetection analysis at a given frequency Ω is a result of the beat note between the intense oscillating field at frequency mode ω, defined as the carrier, and the pair of

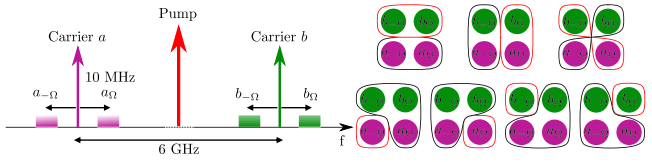

FIG. 1. Representation of frequency sidebands surrounding their corresponding mode carriers "a" and "b." The figure on the right shows all seven possible bipartitions that need to be analyzed with the Simon criteria.

frequency modes at $\omega \pm \Omega$, defined as the sidebands (see Fig. 1). The detailed entanglement structure of the four sideband modes requires a more sophisticated analysis based on the Simon version of positivity under partial transposition (PPT) [18] criteria, which is stated in terms of the symplectic eigenvalues of the partially transposed (PT) covariance matrix reconstructed from experimental data [17]. According to this criteria, there is entanglement between two bipartitions in the system if the smallest symplectic eigenvalue is less than one. Thus, an analysis of all possible bipartitions in the system reveals the entanglement structure between the modes.

The experimental setup is shown in Fig. 2 with a detailed description presented in the Supplemental Material [19]. The OPO consists of a bow-tie cavity with high reflectivity mirrors and a free spectral range (FSR) of 404.7(3) MHz, allowing for a doubly resonant operation between a pair of beams separated by a frequency of 6 GHz, which corresponds to twice the ground state hyperfine atomic splitting of ^{85}Rb. A ^{85}Rb vapor cell with antireflection coatings is placed inside the cavity and is heated to 97 °C for high optical density, as needed for an efficient FWM process.

The pump beam is collinear with the cavity mode and is injected with a polarizing beam splitter PBS_1 and removed by PBS_2. The pump is generated with a Ti:sapphire laser tuned close to the D1 (@795 nm) line of ^{85}Rb, and its frequency is stabilized such that it has a detuning

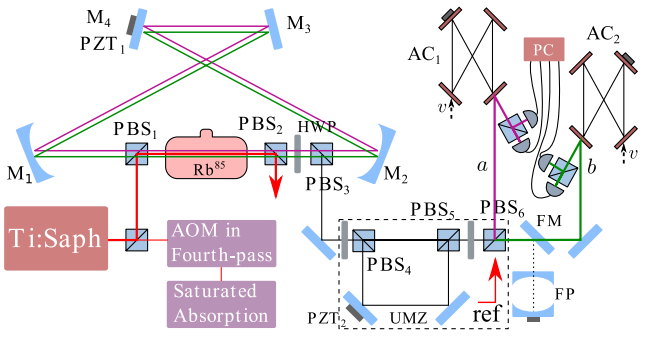

FIG. 2. Sketch of the experimental setup. Mirror (M), confocal Fabry-Perot (FP), flip mirror (FM), analysis cavity (AC), piezoelectric actuator (PZT), and demodulating chain and data acquisition (PC). Other definitions are given in the text.

$\Delta_1 = 0.82$ GHz to the blue of the $5^2S_{1/2}F = 2 \rightarrow 5^2P_{1/2}F = 3$ transition. A half wave-plate (HWP) and PBS_3 are used in order to control the output coupling of the cavity, which has a finesse that ranges from 5 to 30 for a field far from atomic resonance. Since the generated fields are degenerated in polarization, they are separated with an unbalanced Mach-Zehnder (UMZ) interferometer [25], with a discrimination efficiency of 98%.

After spatial separation, we use the technique of resonator detection (RD) [17] to reconstruct the full covariance matrix. The RD technique consists on using the dispersive properties of an optical resonator close to resonance. The analysis cavity leads to a distinct phase shift of the sideband modes before photodetection that depends on its detuning, this enables a full reconstruction of the covariance matrix. After the balanced detection for each beam, the photocurrent is split in two, demodulated using in-quadrature signals at a chosen analysis frequency and processed in a computer. The whole system has an overall detection efficiency of 91%, accounting for optical losses and photodetector quantum efficiency. This process allows for a complete tomography of the quantum state.

As it was already observed for OPOs operating above threshold, the generated quantum state can be described by a Gaussian state, i.e., a stationary state with Gaussian statistics [26]. In this case, the covariance matrix is a faithful description of the Wigner function of the state, and therefore an equivalent mapping of the density operator that contains all the relevant information about the state. In terms of the quadrature operators, the covariance matrix is given by

$$\mathbf{V} = \frac{1}{2}(\langle \vec{X} \cdot \vec{X}^T \rangle + \langle \vec{X} \cdot \vec{X}^T \rangle^T), \tag{2}$$

with

$$\vec{X} = (\hat{p}_{a,-\Omega}, \hat{q}_{a,-\Omega}, \hat{p}_{a,\Omega}, \hat{q}_{a,\Omega}, \hat{p}_{b,-\Omega}, \hat{q}_{b,-\Omega}, \hat{p}_{b,\Omega}, \hat{q}_{b,\Omega})^T,$$

where the operators associated with the amplitude ($\hat{p} = \hat{a} + \hat{a}^\dagger$) and phase [$\hat{q} = -i(\hat{a} + \hat{a}^\dagger)$] quadratures of the sidebands ($\Omega, -\Omega$) of the intense fields (labeled a and b) are arranged from smallest to largest mode frequency (as seen in Fig. 1). The detailed process of state tomography needed to reconstruct the covariance matrix is presented in the Supplemental Material [19].

A first overview of the entanglement structure can be obtained through the usual direct analysis picture based on the spectral components of the photocurrents at a given analysis frequency [3]. In this case, detection with the analysis cavity will measure a linear combination of the sidebands, as is the case for homodyne detection [17]. This is equivalent to writing the covariance matrix in terms of the symmetric combination of sideband modes. In this case, the observed operators associated with the beam a are

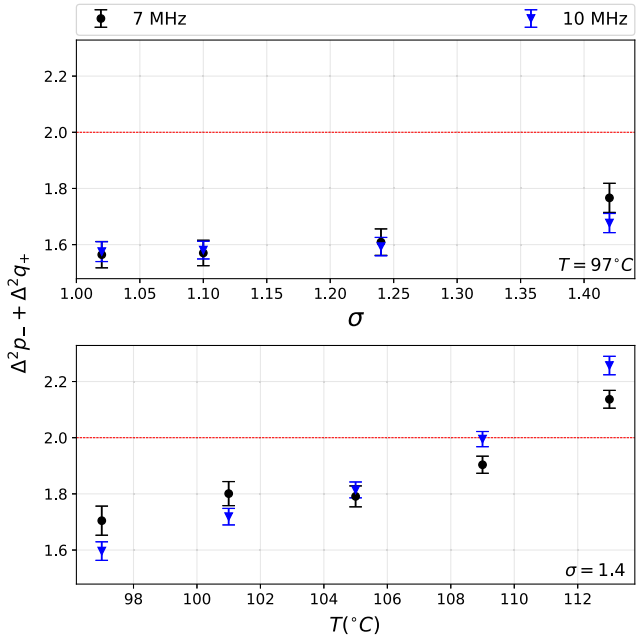

FIG. 3. Top: Duan criterion as a function of $\sigma = P/P_{\mathrm{Th}}$ with $P_{\mathrm{Th}} = 199$ mW. Bottom: Duan Criterion as a function of temperature. The threshold power evolves as $P_{\mathrm{Th}} = 174$, 125, 90, 61.8, 50 mW for $T = 97$, 101, 105, 109, and 113 °C, respectively. For both figures, we consider analysis frequencies of 7 (black circles) and 10 MHz (blue triangles) for a cavity with $\mathcal{F} = 15$. Values less than 2 indicate the presence of entanglement.

$\hat{p}_a = (\hat{p}_{a,\Omega} + \hat{p}_{a,-\Omega})/\sqrt{2}$ and $\hat{q}_{(a)} = (\hat{q}_{a,\Omega} + \hat{q}_{a,-\Omega})/\sqrt{2}$. Together with the corresponding expressions for the output beam b, we can apply the Duan criterion to test for entanglement between the intense beams [16].

We compute the variances given in Eq. (1) for analysis frequencies of 7 and 10 MHz as a function of the pump power normalized to the oscillation threshold power $\sigma = P/P_{Th}$ for $T = 97$ °C, as depicted in Fig. 3 (top). In order to demonstrate a violation of Eq. (1), we compute $\Delta^2\hat{p}_-$ and $\Delta^2\hat{q}_+$ separately, with minimum values of $\Delta^2\hat{p}_- = 0.71(14)$ and $\Delta^2\hat{q}_+ = 0.85(14)$. While amplitude difference squeezing was already shown in [11], the observation of phase sum squeezing for the first time in this kind of OPO gives a clear demonstration of entanglement in the intense generated fields. We show a maximum violation in the Duan criterion of $\Delta^2\hat{p}_- + \Delta^2\hat{q}_+ = 1.56(14) \ngeq 2$. Unlike a solid state OPO, in which phonon noise degrades the squeezing in the phase quadrature [27], atoms do not introduce such excess noise. The violation remains robust as we increase the pump power, and the slight reduction in the violation of the Duan criterion is compatible with the coupling of the pump mode into the doubly resonant OPO, as described in [12]. On the other hand, since the analysis frequencies are smaller than the OPO bandwidth of 27 MHz for this configuration, we do not see a clear dependency on the analysis frequency. It is interesting to notice that the cavity finesse ($\mathcal{F} = 15$) is almost 1 order of magnitude smaller that those usually used for experiments with solid state OPOs [3,8]. This is possible due to the large control over the gain possible with the atomic-based amplifier.

This makes the $\chi^{(3)}$ OPO based on atomic media a versatile source for the generation of a high level of entanglement when operating above threshold, in addition to being more robust against the degradation of phase correlations. Nevertheless, this advantage should be treated with care. We also compute the Duan criterion as a function of temperature in Fig. 3 (bottom) and show that entanglement is degraded until the violation is lost for values higher than 109 °C. While an increase in temperature increases the gain of the medium, thus reducing the threshold power, the spectral broadening of the absorption profile increases the losses, which degrades the entanglement.

Therefore, there is an optimal condition for which we have enough atoms for a fairly low oscillation threshold thanks to the high gain, but avoiding a dense, temperature broadened sample that leads to incoherent effects that degrade the quantum correlations. It is worth noting that in solid state OPOs temperature changes mainly affect the phase quadrature; however, for atomic based parametric amplifiers an increase in temperature leads to an increase in number density and thus absorption. This results in the degradation of correlations in both the amplitude and phase quadratures.

A richer structure of entanglement can be observed for the complete four mode state described by the covariance matrix defined in Eq. (2). Taking the covariance matrix for our state, we can apply now the Simon criteria [18], by calculating the smallest symplectic eigenvalue ν after a partial transposition for all seven possible bipartitions, as shown in Fig. 1. First, we compute ν as a function of the normalized pump power σ for three different values of the finesse ($\mathcal{F} = 13$, 15, 17) for an analysis frequency of 10 MHz and a constant temperature of 97 °C with the results shown in Fig. 4. Values of ν smaller than 1 indicates the presence of an entangled bipartition.

The particular bipartition $(\hat{a}_{-\Omega}, \hat{a}_{+\Omega})$ vs $(\hat{b}_{-\Omega}, \hat{b}_{+\Omega})$ is entangled as expected from the Duan criterion between modes "a" and "b," and presents the maximal violation of all possible bipartitions. It is interesting to note that the other 2×2 bipartitions have a quite different behavior. While bipartition $(\hat{a}_{-\Omega}, \hat{b}_{-\Omega})$ vs $(\hat{a}_{+\Omega}, \hat{b}_{+\Omega})$, which involves the correlation between the lower against the upper sidebands presents a violation almost as strong as the one between the two bright beams, the bipartition $(\hat{a}_{-\Omega}, \hat{b}_{+\Omega})$ vs $(\hat{a}_{+\Omega}, \hat{b}_{-\Omega})$ is compatible with a separable state. This is consistent with the sideband picture in which we have a pair of two mode squeezing operators, acting on the modes $(\hat{a}_{-\Omega}, \hat{b}_{+\Omega})$ and $(\hat{a}_{+\Omega}, \hat{b}_{-\Omega})$ independently [12].

We consider now the entanglement of a single sideband against the remaining set of modes, e.g., $(\hat{a}_{-\Omega})$ vs

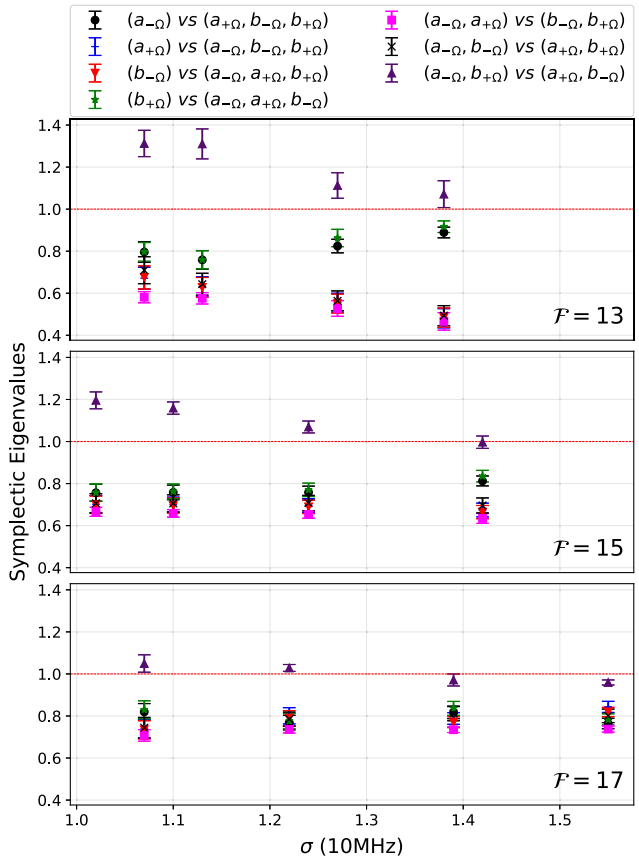

FIG. 4. Smallest symplectic eigenvalues for all possible bipartitions after partial transposition as a function of σ, the pump power normalized to the threshold power. For all data we use an analysis frequency of 10 MHz and a temperature of 97 °C for $\mathcal{F} = 13$, 15, 17, which leads to $P_{\mathrm{Th}} = 274$, 199, 138 mW, respectively.

$(\hat{a}_{+\Omega}, \hat{b}_{-\Omega}, \hat{b}_{+\Omega})$. It is interesting to note that in an open cavity ($\mathcal{F} = 13$), the degree of entanglement between different bipartitions is far from being symmetric. For instance, Fig. 4 shows that at $\sigma \sim 1.4$, for the internal modes $\hat{a}_{+\Omega}$ (blue cross) and $\hat{b}_{-\Omega}$ (downward red triangle), the symplectic eigenvalues are near 0.5; whereas for the modes $\hat{a}_{-\Omega}$ (black circle) and $\hat{b}_{+\Omega}$ (green star) the symplectic eigenvalues are near 0.9. However, this asymmetry tends to disappear gradually as the finesse increases. For $\mathcal{F} = 17$, the symplectic eigenvalues in the four 1×3 bipartitions all tend to the same value around 0.8. The interplay between the asymmetric gain medium spectral profile [28] and the symmetric cavity response in frequency plays a role that requires a detailed treatment beyond the one we presented in [12].

The observed entanglement is dependent on the temperature, as can be observed by exploring this parameter for an analysis frequency of 10 MHz, $\sigma = 1.42$, and $\mathcal{F} = 15$, as shown in Fig. 5. Atomic density is a determinant factor for the generation and degradation of entanglement, in a similar way as that observed for the Duan criterion.

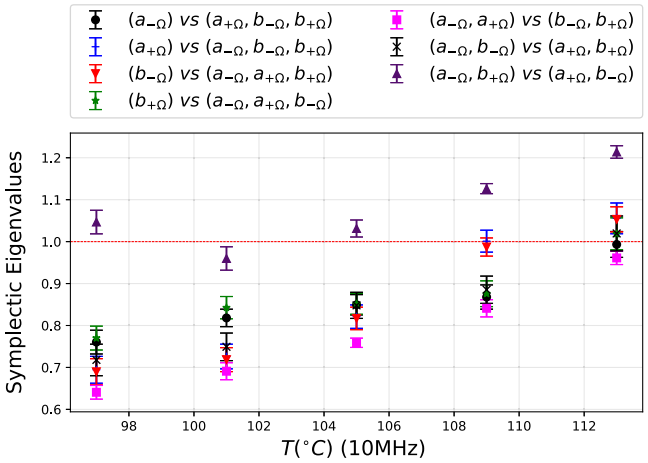

FIG. 5. Smallest symplectic eigenvalues for all possible bipartitions after partial transposition as a function of temperature. For all data, we use an analysis frequency of 10 MHz and $\sigma = 1.42$ for $T = 97$, 101, 105, 109, 113 °C, which leads to $P_{\mathrm{Th}} = 174$, 125, 90, 61.8, 50 mW, respectively.

For a temperature of 97°C the entangled bipartitions all show a violation of the Simon criteria with their smallest symplectic eigenvalues near 0.7; however, the entanglement is lost when the temperature is increased to 113 °C. A more detailed characterization of the entanglement structure of the four mode system is obtained when we analyze the entanglement for bipartitions composed of individual modes against the remaining modes. Figure 5 shows that internal bands $\hat{a}_{+\Omega}$ (blue cross) and $\hat{b}_{-\Omega}$ (downward red triangle) exhibit a similar behavior, having more entanglement than external bands $\hat{a}_{-\Omega}$ (black circle) and $\hat{b}_{+\Omega}$ (green star) at low temperature values. When the temperature increases this behavior flips and external bands have more entanglement than internal ones until finally entanglement is lost.

As we have demonstrated, an OPO based on a nonlinear FWM process in a hot atomic vapor produces entangled twin beams with an entanglement structure that is consistent with the production of two-mode entangled states involving pairs of sidebands of the signal and idler modes. The absence of phonon noise in the gain medium is an advantage over other OPO configurations based on a $\chi^{(2)}$ or $\chi^{(3)}$ process in solids. The extremely high gain possible with an atomic medium allows for the use of a cavity with low finesse, which results in a high escape rate for the produced fields. Additionally, the combination of an adjustable amplifier and a versatile cavity allows for the engineering of the generated modes. With simple improvements, a dedicated setup can be used to produce higher levels of entanglement that may compete with the best values obtained by a $\chi^{(2)}$ OPO. Some limitations, nevertheless, are present. Atomic density, controlled by the temperature of the ^{85}Rb vapor cell, is an important parameter that degrades the correlations in the system and can lead to the loss of entanglement. This does not change the fact that

the system is a rich and useful tool for the generation of quantum multipartite entangled states that are close to atomic resonance, with applications in many aspects of quantum information.

This work was funded by Grants No. 2015/18834-0, 2017/27216-4 and No. 2018/03155-9 São Paulo Research Foundation (FAPESP), and Grant No. N629091612184 (NICOP/ONR).

*amontanag@usp.br
†hans@if.usp.br

[1] M. A. Nielsen and I. L. Chuang, *Quantum Computation and Quantum Information* (Cambridge University Press, Cambridge, England, 2011).
[2] Z. Y. Ou, S. F. Pereira, H. J. Kimble, and K. C. Peng, Phys. Rev. Lett. **68**, 3663 (1992).
[3] A. S. Villar, L. S. Cruz, K. N. Cassemiro, M. Martinelli, and P. Nussenzveig, Phys. Rev. Lett. **95**, 243603 (2005).
[4] M. Pysher, Y. Miwa, R. Shahrokhshahi, R. Bloomer, and O. Pfister, Phys. Rev. Lett. **107**, 030505 (2011).
[5] O. Pinel, P. Jian, R. M. de Araújo, J. Feng, B. Chalopin, C. Fabre, and N. Treps, Phys. Rev. Lett. **108**, 083601 (2012).
[6] Shota Yokoyama, Ryuji Ukai, Seiji C. Armstrong, Chanond Sornphiphatphong, Toshiyuki Kaji, Shigenari Suzuki, Junichi Yoshikawa, Hidehiro Yonezawa, Nicolas C. Menicucci, and Akira Furusawa, Nat. Photonics **7**, 982 (2013).
[7] M. Chen, N. C. Menicucci, and O. Pfister, Phys. Rev. Lett. **112**, 120505 (2014).
[8] Avik Dutt, Kevin Luke, Sasikanth Manipatruni, Alexander L. Gaeta, Paulo Nussenzveig, and Michal Lipson, Phys. Rev. Appl. **3**, 044005 (2015).
[9] C. F. McCormick, V. Boyer, E. Arimondo, and P. D. Lett, Opt. Lett. **32**, 178 (2007).
[10] A. M. Marino, V. Boyer, and P. D. Lett, Phys. Rev. Lett. **100**, 233601 (2008).
[11] A. M. Guerrero, P. Nussenzveig, M. Martinelli, A. M. Marino, and H. M. Florez, Phys. Rev. Lett. **125**, 083601 (2020).
[12] Barbara Abigail Ferreira Ribeiro, R. B. de Andrade, M. Martinelli, and B. Marques, Phys. Rev. A **102**, 023522 (2020).
[13] Da Zhang, Changbiao Li, Zhaoyang Zhang, Yiqi Zhang, Yanpeng Zhang, and Min Xiao, Phys. Rev. A **96**, 043847 (2017).
[14] Y. Cai, J. Roslund, G. Ferrini, F. Arzani, X. Xu, C. Fabre, and N. Treps, Nat. Commun. **8**, 15645 (2017).
[15] A. Lvovsky, B. Sanders, and W. Tittel, Nat. Photonics **3**, 706 (2009).
[16] Lu-Ming Duan, Géza Giedke, Juan Ignacio Cirac, and Peter Zoller, Phys. Rev. Lett. **84**, 2722 (2000).
[17] F. A. S. Barbosa, A. S. Coelho, K. N. Cassemiro, P. Nussenzveig, C. Fabre, A. S. Villar, and M. Martinelli, Phys. Rev. A **88**, 052113 (2013).
[18] R. Simon, Phys. Rev. Lett. **84**, 2726 (2000).
[19] See Supplemental Material at http://link.aps.org/supplemental/10.1103/PhysRevLett.129.163601, which includes Refs [11,16–18,20–24] for details of the experimental setup, covariance matrix reconstruction with the resonator detection technique, and entanglement test.
[20] F. A. S. Barbosa, A. S. Coelho, K. N. Cassemiro, M. Martinelli, P. Nussenzveig, and A. S. Villar, Phys. Rev. A **102**, 063705 (2020).
[21] F. A. S. Barbosa, A. S. Coelho, L. F. Muñoz-Martinez, L. Ortiz-Gutiérrez, A. S. Villar, P. Nussenzveig, and M. Martinelli, Phys. Rev. Lett. **121**, 073601 (2018).
[22] E. Schrödinger, Ber. Kgl. Akad. Wiss. Berlin **24**, 296 (1930).
[23] H. P. Robertson, Phys. Rev. **46**, 794 (1934).
[24] R. F. Werner and M. M. Wolf, Phys. Rev. Lett. **86**, 3658 (2001).
[25] E. H. Huntington, G. N. Milford, C. Robilliard, T. C. Ralph, O. Glöckl, U. L. Andersen, S. Lorenz, and G. Leuchs, Phys. Rev. A **71**, 041802 (2005).
[26] A. S. Coelho, F. A. S. Barbosa, K. N. Cassemiro, M. Martinelli, A. S. Villar, and P. Nussenzveig, Phys. Rev. A **92**, 012110(R) (2015).
[27] A. S. Coelho, F. A. S. Barbosa, K. N. Cassemiro, A. S. Villar, M. Martinelli, and P. Nussenzveig, Science **326**, 823 (2009).
[28] Q. Glorieux, R. Dubessy, S. Guibal, L. Guidoni, J.-P. Likforman, T. Coudreau, and E. Arimondo, Phys. Rev. A **82**, 033819 (2010).